Palladium Single Atoms on TiO2 as a Photocatalytic Sensing Platform for Analyzing Organophosphorus Pesticide Chlorpyrifos

Article *in* Angewandte Chemie International Edition · October 2019

DOI: 10.1002/anie.201911516

Peng Zhou
University of Michigan

Shulin Chen
Harbin Institute of Technology

Shaojun Guo
Brown University

VIP Single-Atom Catalysis Very Important Paper

International Edition: DOI: 10.1002/anie.201911516
German Edition: DOI: 10.1002/ange.201911516

Palladium Single Atoms on TiO_2 as a Photocatalytic Sensing Platform for Analyzing the Organophosphorus Pesticide Chlorpyrifos

*Xiaoxiao Ge[+], Peng Zhou[+], Qinghua Zhang, Zhonghong Xia, Shulin Chen, Peng Gao, Zhe Zhang, Lin Gu, and Shaojun Guo**

Abstract: *Traditional methods for analyzing organophosphorus pesticide chlorpyrifos, usually require the tedious sample pretreatment and sophisticated bio-interfaces, leading to the difficulty for real-time analysis. Herein, we use palladium single-atom (PdSA)/TiO_2 as a photocatalytic sensing platform to directly detect chlorpyrifos with high sensitivity and selectivity. PdSA/TiO_2, prepared by an in situ photocatalytic reduction of $PdCl_4^{2-}$ on the TiO_2, shows much higher photocatalytic activity (10 mol g^{-1} h^{-1}) for hydrogen evolution reaction than Pd nanoparticles (1.95 mol g^{-1} h^{-1}), and excellent stability. In the presence of chlorpyrifos, the photocatalytic activity of PdSA/TiO_2 decreases. Through this inhibition effect the platform can realize a detection limit for chlorpyrifos of 0.01 ng mL^{-1}, much lower than the maximum residue limit (10 ppb) permitted by the U.S. Environmental Protection Agency.*

Organophosphorus pesticides (OPs) have been historically utilized to eliminate the pests in agricultural industry for high production of crops.[1] However, the residual pesticides easily enter into human body via the uptake of crops and water as well as the atmosphere. Even a small amount of OPs exposed in vivo can rapidly inhibit the activity of cholinesterase enzymes and subsequently block the neurotransmitter transmission, thus leading to the disfunction of nervous system and the subsequent physical discomfort to people, even death.[2,3] Chlorpyrifos is one of the representative OPs, and popularly applied to control the agricultural and house hold pests around the world.[4] The annual consumption of chlorpyrifos in China is up to 18000 tones. The use of chlorpyrifos in such large quantity no doubt lead to the abuse of pesticides. Thus, highly sensitive detection of chlorpyrifos, remained in crops samples and environmental samples, is of vital importance for real-time evaluation of food safety. In terms of chlorpyrifos detection, different analytical methods such as gas/liquid chromatography (GC/LC),[5,6] GC-MS[7,8] and nanomaterials-based biosensors,[9] have been demonstrated by researchers from various fields. However, the previous strategies still face huge challenges despite the great advances made for the time being. For example, GC/LC and GC-MS usually involve tedious sample pretreatment steps. Biosensing interfaces in nano-biosensors still suffer from bottlenecks of short storage time and harsh storage conditions. Thus these problems hamper the real-time output of experimental results for chlorpyrifos residues to some extent.

Single-atom (SA) catalysts, a newcomer in the field of nanocatalysis, have garnered increasing attention of enormous researchers from various disciplines.[10] Compared with the conventional catalysts with the size of nanoparticles or nanoclusters, SA catalysts exhibit the atomically dispersed active sites on the support that endows them the optimum atomic utilization efficiency, the excellent electron properties as well as the enhanced catalytic activity.[11,12] The unique features make SA catalysts be ideal model to understand the catalytic mechanism at the molecule level, simultaneously bridging the gap between homogeneous catalysis and heterogeneous catalysis.[13] Current researches on SA catalysts are mainly centered on the energy-related field, such as electro-

[*] X. X. Ge,[+] P. Zhou,[+] Z. H. Xia, Prof. S. J. Guo
Department of Materials Science & Engineering, College of Engineering, Peking University
Beijing 100871 (China)
E-mail: guosj@pku.edu.cn
Q. H. Zhang, Prof. L. Gu
Beijing National Laboratory for Condensed Matter and Institute of Physics, Chinese Academy of Sciences
Beijing 100190 (China)
and
School of Physical Sciences, University of Chinese Academy of Sciences
Beijing 100049 (China)
S. L. Chen, Prof. P. Gao
Electron Microscopy Laboratory, and International Center for Quantum Materials, School of Physics, Peking University
Beijing 100871 (China)
S. L. Chen
State Key Laboratory of Advanced Welding and Joining, Harbin Institute of Technology
Harbin 150001 (China)
Prof. P. Gao
Collaborative Innovation Centre of Quantum Matter
Beijing 100871 (China)
Z. Zhang
Institute of Environmental Research at Greater Bay Area; Key Laboratory for Water Quality and Conservation of the Pearl River Delta, Ministry of Education, Guangzhou University
Guangzhou 510006 (China)
Prof. S. J. Guo
BIC-ESAT, College of Engineering, Peking University
Beijing 100871 (China)
and
Department of Energy and Resources Engineering, College of Engineering, Peking University
Beijing 100871 (China)
[+] These authors contributed equally to this work.
Supporting information and the ORCID identification number(s) for the author(s) of this article can be found under: https://doi.org/10.1002/anie.201911516.

catalyst and photocatalyst.[14,15] Previous reports have fully demonstrated the extraordinary activity and stability of SA catalysts in hydrogen evolution reaction (HER),[16,17] oxygen reduction reaction (ORR),[18] and oxygen evolution reaction (OER).[19] Despite booming growth regarding energy-related application, the bioapplication of SA catalysts is still in its infancy,[20,21] and SA catalyst applied for detection of pesticides residues was never reported until now.

Herein, we first adopt PdSA supported TiO_2 as an advanced photocatalytic sensing platform for highly sensitive detection of chlorpyrifos via restricting the photocatalytic H_2 evolution activity of PdSA by chlorpyrifos. Benefiting from the highly uniform and atomic dispersion of Pd active sites, PdSA/TiO_2 exhibits the much enhanced photocatalytic HER performance and adequate sensitivity for chlorpyrifos determination. Without any complex pre-processing procedures, such a method is less time-consuming and direct, providing great potential for environmental monitoring chlorpyrifos residues.

The SA catalyst of Pd/TiO_2 was prepared by an in situ photocatalytic reduction strategy under the iced state. The homogeneous mixture solution of TiO_2 and Pd precursors (K_2PdCl_4) was treated with liquid nitrogen to form an ice bulk. The strong interaction between the electron-rich oxygen of TiO_2 and the empty orbitals of the metal Pd, deposited the $PdCl_4^{2-}$ on the surface of TiO_2 nanoparticles. Irradiation with Xe light of the ice bulk, excited TiO_2 to produce photogenerated electrons that subsequently promoted the reduction of $PdCl_4^{2-}$ to form metal Pd species, giving Pd_1/TiO_2. As a control, the same mixture, but without the freezing process was directly irradiated by Xe light, to give Pd_2/TiO_2.

Transmission electron microscope (TEM), scanning transmission electron microscope (STEM)-energy dispersive X-ray spectroscopy (EDS) and the aberration-corrected high-angle annular dark-field (HAADF)-STEM were applied to characterize the morphology of the as-made Pd species. TEM images demonstrate that there are many small dots on the surface of Xe light-irradiated TiO_2, Pd_1/TiO_2 and Pd_2/TiO_2 (Figure S1 in the Supporting Information) when compared with the untreated TiO_2. The results from STEM-EDS and the HAADF-STEM characterizations clearly show that metal Pd in Pd_1/TiO_2 sample is uniformly dispersed onto TiO_2 substrate (Figure 1 a,b). The X-ray absorption near-edge structure (XANES) spectroscopy of Pd_1/TiO_2 with atomic dispersion show a slightly higher energy for the absorption edge than that of Pd foil (Figure 1 d), suggesting the presence of oxidized Pd. Furthermore, the Pd K-edge spectra in extended X-ray adsorption fine structure (EXAFS) analysis emerge a sharp characteristic peak of Pd–O bond (in the region of 1 Å to 2 Å) and a weak peak of Pd–Pd (Figure 1 c), fully confirming the subjective status of PdSA on TiO_2 substrate after the iced treatment. In X-ray diffraction (XRD) characterization, Pd_1/TiO_2 does not exhibit any peak of Pd nanoparticles when compared with Pd_2/TiO_2 sample (Figure S2), further demonstrating that PdSA with the ultra-small size has no significant effect on the structure of TiO_2. Thus, Pd_1/TiO_2 is called PdSA/TiO_2 while Pd_2/TiO_2 is named for Pd nanoparticles/TiO_2 (PdNPs/TiO_2). The Pd contents in PdSA/TiO_2 and PdNPs/TiO_2 were determined to be 0.53 wt % and 0.56 wt %, respectively via the inductively coupled plasma-atomic emission spectroscopy (ICP-AES).

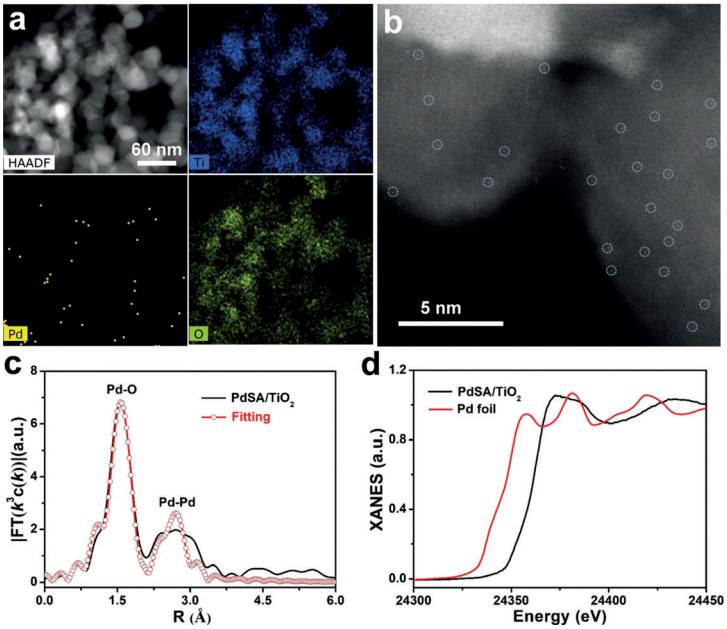

Figure 1. The structural characterizations of PdSA/TiO_2. a) EDS-STEM elemental mapping and b) HAADF-STEM image of PdSA/TiO_2, c) Fourier transform of the Pd K-edge of the EXAFS spectra of PdSA/TiO_2, d) normalized XANES spectra at the Pd L3-edge of PdSA/TiO_2 and Pd foil.

Figure 2 a shows the schematic principle on photocatalytic HER of PdSA/TiO_2. Under the irradiation of visible light, the electrons from valence band of TiO_2 was excited into the

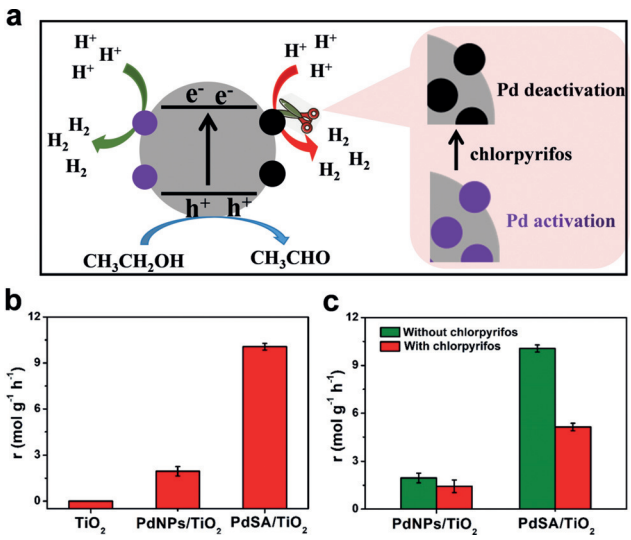

Figure 2. a) The principle of the PdSA/TiO_2-based sensing platform utilizing photocatalytic H_2 production; b) The photocatalytic H_2 production rate of PdSA/TiO_2 and PdNPs/TiO_2; c) The inhibition behavior of chlorpyrifos on the photocatalytic HER performance of both PdSA/TiO_2 and PdNPs/TiO_2.

conduction band that directly reacted H^+ in the solution to generate H_2 through PdSA. Meanwhile, the generated positive charged hole (h^+) promoted the oxidation of ethanol to form acetaldehyde. Figure 2b displays the photocatalytic performance of PdSA/TiO_2 and PdNPs/TiO_2. As expected, the TiO_2 support substrate, did not present any photocatalytic HER signal due to the lack of metal Pd. PdSA/TiO_2 exhibits the remarkably enhanced photocatalytic performance with the H_2 production rate of up to 10 mol $g^{-1}h^{-1}$, much higher than that of PdNPs/TiO_2 (1.95 mol $g^{-1}h^{-1}$). Such an excellent photocatalytic performance generated at a lower loading level of Pd further suggested the super-high density and active sites of PdSA on TiO_2 substrate in comparison to PdNPs. Most importantly, we unexpectedly discover that in the presence of chlorpyrifos, the photocatalytic HER activity of PdSA/TiO_2 is significantly inhibited whereas that of PdNPs/TiO_2 did not exhibit any observed change (Figure 2a,c). Though both PdSA/TiO_2 and PdNPs/TiO_2 have the similar loading amount of Pd element, PdSA exhibited much higher dispersion of Pd active sites due to the ultimately atomic utilization efficiency than PdNPs. Chlorpyrifos is prone to block the photocatalytic HER active sites of PdSA, thus suggesting that PdSA/TiO_2 is more sensitive toward chlorpyrifos.

X-ray photoelectron spectra (XPS) and mass spectra (MS) were employed to characterize the interaction between chlorpyrifos and PdSA/TiO_2. Figure 3 displays the XPS spectra of Pd 3d. For the as-synthesized PdSA/TiO_2, the binding energies of Pd0 3d at 341.28 ($3d_{3/2}$) eV and 336.08 eV ($3d_{5/2}$) exhibit slight difference from the standard values of bulk Pd ($3d_{3/2}$ = 341.1 eV; $3d_{5/2}$ = 335.2 eV) because of the interaction between Pd species and TiO_2. In the meantime, the peaks in XPS spectrum of Pd 3d at 342.48 eV and 337.18 eV typically verify the existence of oxidized Pd^{II} (Figure 3a), being in good agreement with the XANES result. In XPS analysis of the PdSA/TiO_2 exposed to chlorpyrifos, both the peaks of Pd $3d_{3/2}$ and Pd $3d_{5/2}$ show noticeable negative shift compared with that of the unexposed PdSA/TiO_2 owing to the adsorption of chlorpyrifos with electron-rich group on the electron-withdrawing PdSA/TiO_2 (Figure 3b). This typical XPS feature of Pd 3d before and after chlorpyrifos exposure is highly in accordance with the previous report on the strong interaction of Pd^{II} with sulfur-containing compound or nanomaterials.[22,23] In MS analysis, $Pd(CH_3CN)_4(BF_4)_2$ was used here as Pd^{II} species to react with chlorpyrifos. One peak with 1^+ charge state is observed in electrospray ionization mass spectrometry (ESI-MS), due to loss of the counterion, BF_4^-. After deconvolution of m/z, the average measured composition of S1 is 977.76 Da, which exactly agreeing with the molecular composition of S1 $[(C_9H_{11}Cl_3NO_3PS)_2Pd(BF_4)_2]$. The corresponding fragmentation masses are around 890.76 (Figure S3), indirectly confirming the strong interaction of chlorpyrifos with PdSA on TiO_2 supports.

The developed PdSA/TiO_2-based photocatalytic sensing platform provides a direct and simple strategy for chlorpyrifos determination. Some certain parameters were explored subsequently to evaluate the reliability of this method. As shown in Figure S4, the photocatalytic H_2 production rate of PdSA/TiO_2 rapidly increases in the first 10 min of Xe light irradiation and reaches a plateau at 30 min. Hence, 30 min is the optimal time selected to perform this photocatalytic reaction. Besides, the reaction time of 30 min implies that this approach is adequate to realize the real-time detection of chlorpyrifos residues. The photocatalytic stability of PdSA/TiO_2 was also investigated in detail. The synthesized PdSA/TiO_2 was stored in the centrifuged tube at room temperature, and tested every two months. It is demonstrated that the photocatalytic H_2 production rate of PdSA/TiO_2 retains the initiate level well even after eight months (Figure S5). Especially, the same dose of chlorpyrifos still realizes the same inhibition effect on the photocatalytic performance of PdSA/TiO_2 (Figure 4a). These results underscore the excellent stability of PdSA/TiO_2-based photocatalytic sensor as well as the favorable prospect toward chlorpyrifos analysis. Inspired by the above results, this PdSA/TiO_2-based photocatalytic sensing strategy was then applied to detect different concentrations of chlorpyrifos standard samples. The resulting photocatalytic H_2 production rate decrease with increasing chlorpyrifos content in the samples from 0.03 ng mL^{-1} to 10 μg mL^{-1} (Figure 4b). The detection of limit is determined to be lower to 0.01 ng mL^{-1}, much lower than those of the previously reported methods.[24,25] Moreover, according to the report from U.S. Environment Protection Agency, the maximum residues amount of chlorpyrifos in nearly all the agriculture products has to be lower than 10 ppb.[26] Thus, our proposed photocatalytic sensing platform features the remarkable sensitivity for chlorpyrifos determination.

Three other OPs commonly used in crop protection, including paraoxon-ethyl, monocrotophos, and dipterex were examined to evaluate the selectivity of this method. The results showed that these other pesticides did not cause any obvious inhibition effect on the photocatalytic activity of PdSA/TiO_2 (Figure 4c). Moreover, some anions and cations that are ubiquitous on vegetables and crops have been successfully verified to have no influence on the photocatalytic performance of PdSA/TiO_2 (Figure 4d), significantly certifying the reliability of the proposed method for chlorpyrifos assay. Spinach was used here as the model vegetable to explore the practical use of this sensing platform. The results achieved demonstrate that the vegetable samples

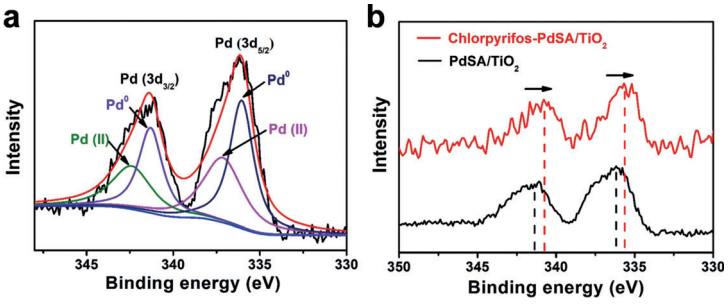

Figure 3. XPS of a) Pd 3d from PdSA/TiO_2 and b) Pd 3d XPS of PdSA/TiO_2 before and after the reaction with chlorpyrifos.

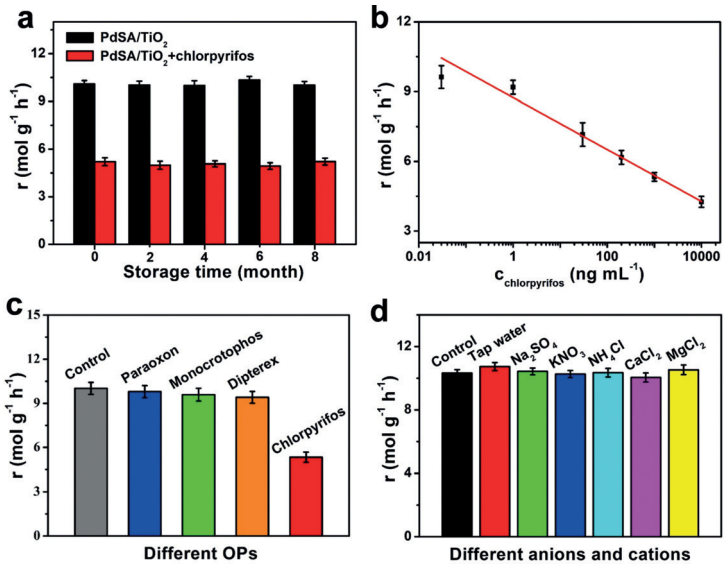

Figure 4. a) The photocatalytic HER stability of PdSA/TiO_2 before and after the introduction of chlorpyrifos. b) The typically photocatalytic response of PdSA/TiO_2 toward different concentrations of chlorpyrifos, 0.03 ng mL^{-1}, 1 ng mL^{-1}, 30 ng mL^{-1}, 200 ng mL^{-1}, 1 μg mL^{-1}, 10 μg mL^{-1}. c) The interference assessment of other commonly used organophosphorus pesticides on chlorpyrifos determination. d) The interference analysis of the anions and cations common in vegetable samples.

before and after spiking with chlorpyrifos exhibit distinct inhibition behaviors to the photocatalytic activity of PdSA/TiO_2, with the average recovery rate of 125 % (Figure S6 and Table 1), exhibiting the acceptable practicability for real-time assay of chlorpyrifos residues.

Table 1: Recovery measurement of chlorpyrifos-spiked vegetable samples by PdSA/TiO_2-based photocatalytic sensing platform.[a]

Property	Sample number				
	1	2	3	4	5
Chlorpyrifos spiked (ng/mL)	0	5	50	200	1000
Chlorpyrifos detected (ng/mL)	0.03	6.9	62	238	1200
Recovery (%)	–	138	124	119	120

[a] (ng/mL) indicates ng of chlorpyrifos to mL of 25 % ethanol aqueous solution.

In conclusion, we developed an advanced photocatalytic sensing platform that employed SA catalysts of PdSA/TiO_2 for direct and simple chlorpyrifos detection. HAADF-STEM and XANES characterizations fully confirmed the monoatomic feature of as-made PdSA/TiO_2. PdSA/TiO_2, owing to their high number of active sites, displayed much higher photocatalytic HER performance than PdNPs/TiO_2. Most especially, the presence of chlorpyrifos has a more pronounced inhibition effect on the photocatalytic activity of PdSA/TiO_2 in comparison to PdNPs/TiO_2. The PdSA/TiO_2-based photocatalytic sensing platform achieves a good linear relationship ranged from 0.03 ng mL^{-1} to 10 μg mL^{-1} chlorpyrifos with a very low detection limit of 0.01 ng mL^{-1}. Moreover, both the commonly existing ions and other generally used OPs (paraoxon, monocrotophos and dipterex) did not interfere with chlorpyrifos determination, indicative of the good selectivity of PdNPs/TiO_2-based sensing of chlorpyrifos. For chlorpyrifos-spiked spinach samples, the proposed sensing method exhibited definite feasibility with the average recovery rate of 125 %. This typical SA catalyst-based photocatalytic sensing platform opens up a new pathway for chlorpyrifos residual detection, providing the prospect for exploring novel biosensing strategies for OPs.

Acknowledgements

This work was financially supported by the Beijing Natural Science Foundation (No. JQ18005), National Key R&D Program of China (No. 2016YFB0100201), National Natural Science Foundation of China (No. 51671003), BIC-ESAT funding, and the China Postdoctoral Science Foundation (No. 2018M630021).

Conflict of interest

The authors declare no conflict of interest.

Keywords: chlorpyrifos detection · hydrogen evolution reaction · photocatalysis · single-atom catalyst · titanium

How to cite: *Angew. Chem. Int. Ed.* **2020**, *59*, 232–236
Angew. Chem. **2020**, *132*, 238–242

[1] D. K. Nomura, J. K. Casida, *J. Agric. Food Chem.* **2011**, *59*, 2808–2815.
[2] D. Lu, J. Wang, L. Wang, D. Du, C. Timchalk, R. Barry, Y. Lin, *Adv. Funct. Mater.* **2011**, *21*, 4371–4378.
[3] X. Ge, W. Zhang, Y. Lin, D. Du, *Biosens. Bioelectron.* **2013**, *50*, 486–491.
[4] L. Wang, D. Lu, J. Wang, D. Du, Z. Zou, H. Wang, J. N. Smith, C. Timchalk, F. Liu, Y. Lin, *Biosens. Bioelectron.* **2011**, *26*, 2835–2840.
[5] A. Shanker, C. Sood, V. Kumar, S. D. Ravindranath, *Pest Manage. Sci.* **2001**, *57*, 458–462.
[6] S. Samadia, H. Sereshtia, Y. Assadi, *J. Chromatogr. A* **2012**, *1219*, 61–65.
[7] K. Maštovská, S. J. Lehotay, *J. Chromatogr. A* **2004**, *1040*, 259–272.
[8] H. Kataoka, H. L. Lord, J. Pawliszyn, *J. Chromatogr. A* **2000**, *880*, 35–62.
[9] W. Zhang, A. M. Asiri, D. Liu, D. Du, Y. Lin, *TrAC Trends Anal. Chem.* **2014**, *54*, 1–10.
[10] B. Qiao, A. Wang, X. Yang, L. F. Allard, Z. Jiang, Y. Cui, J. Liu, J. Li, T. Zhang, *Nat. Chem.* **2011**, *3*, 634.
[11] J. Qian, Z. Yang, C. Wang, K. Wang, Q. Liu, D. Jiang, Y. Yan, K. Wang, *J. Mater. Chem. A* **2015**, *3*, 13671–13678.
[12] J. Chen, Y. Huang, P. Kannan, L. Zhang, Z. Lin, J. Zhang, T. Chen, L. Guo, *Anal. Chem.* **2016**, *88*, 2149–2155.
[13] W. Hu, Q. Chen, H. Li, Q. Ouyang, J. Zhao, *Biosens. Bioelectron.* **2016**, *80*, 398–404.
[14] Y. Chen, S. Ji, Y. Wang, J. Dong, W. Chen, Z. Li, R. Shen, L. Zheng, Z. Zhuang, D. Wang, Y. Li, *Angew. Chem. Int. Ed.* **2017**, *56*, 6937–6941; *Angew. Chem.* **2017**, *129*, 7041–7045.
[15] W. Zhong, R. Sa, L. Li, Y. He, L. Li, J. Bi, Z. Zhuang, Y. Yu, Z. Zou, *J. Am. Chem. Soc.* **2019**, *141*, 7615–7621.

[16] K. Jiang, B. Liu, M. Luo, S. Ning, M. Peng, Y. Zhao, Y. Lu, T. Chan, F. Groot, Y. Tan, *Nat. Commun.* **2019**, *10*, 1743.
[17] P. Zhou, F. Lv, N. Li, Y. Zhang, Z. Mu, Y. Tang, J. Lai, Y. Chao, M. Luo, F. Lin, J. Zhou, D. Su, S. Guo, *Nano Energy* **2019**, *56*, 127–137.
[18] S. Yang, J. Kim, Y. J. Tak, A. Soon, H. Lee, *Angew. Chem. Int. Ed.* **2016**, *55*, 2058–2062; *Angew. Chem.* **2016**, *128*, 2098–2102.
[19] J. Wang, Z. Li, Y. Wu, Y. Li, *Adv. Mater.* **2018**, *30*, 1801649.
[20] L. Wang, J. Chen, L. Gan, J. Wang, S. Dong, *Sci. Adv.* **2019**, *5*, eaav5490.
[21] L. Jiao, H. Yan, Y. Wu, W. Gu, C. Zhu, D. Du, Y. Lin, *Angew. Chem. Int. Ed.* **2019**, https://doi.org/10.1002/anie.201905645; *Angew. Chem.* **2019**, https://doi.org/10.1002/ange.201905645.
[22] G. Celik, S. Ailawar, S. Gunduz, J. Miller, P. Edmiston, U. Ozkan, *Ind. Eng. Chem. Res.* **2019**, *58*, 4054–4064.
[23] Z. Luo, Y. Ouyang, H. Zhang, M. Xiao, J. Ge, Z. Jiang, J. Wang, D. Tang, X. Cao, C. Liu, W. Xing, *Nat. Commun.* **2018**, *9*, 2120.
[24] Q. Liu, Y. Yin, N. Hao, J. Qian, L. Li, T. You, H. Mao, K. Wang, *Sens. Actuators B* **2018**, *260*, 1034–1042.
[25] H. Li, J. Li, Q. Xu, X. Hu, *Anal. Chem.* **2011**, *83*, 9681–9686.
[26] K. Zhang, Q. Mei, G. Guan, B. Liu, S. Wang, Z. Zhang, *Anal. Chem.* **2010**, *82*, 9579–9586.

Manuscript received: September 9, 2019
Version of record online: November 14, 2019

